JOURNAL OF GEOPHYSICAL RESEARCH, VOL. 111, B11208, doi:10.1029/2005JB004132, 2006

Influence of decompression rate on the expansion velocity and expansion style of bubbly fluids

Atsuko Namiki[1,2] and Michael Manga[1]

Received 29 October 2005; revised 29 June 2006; accepted 15 August 2006; published 22 November 2006.

[1] The decompression rate of magma is correlated with explosivity of volcanic eruptions. We present a series of decompression experiments in a shock tube apparatus to investigate the effect of decompression rate on the expansion and eruption style of bubbly fluids. We also consider the effects of the pressure change ΔP and initial vesicularity ϕ_i. As an analogue for magma we use viscoelastic polymer solutions. For fast decompression, we observe fragmentation and rupture of bubble walls only for large ΔP and large ϕ_i. For slow decompression, however, bubbles maintain spherical shapes, and the bubbly fluid does not fragment, irrespective of ΔP and ϕ_i. We consider two theoretical estimates for the expansion of bubbles, which we refer to as "equilibrium expansion," in which the pressures inside and outside the bubbles are assumed to be equal, and "disequilibrium expansion," in which the enthalpy change caused by the pressure change is converted into kinetic energy. The observed expansion velocity is governed by the slower estimate. For slow decompression, where bubbles expand while maintaining their spherical shape, the measured expansion is well explained by equilibrium expansion. In contrast, for fast decompression, in which we observe the rupture of bubble walls and fragmentation, the expansion follows disequilibrium expansion. We conclude that the disequilibrium estimate is an upper limit velocity for the bubble expansion and fragmentation and the rupture of bubble walls require disequilibrium expansion. The calculated threshold decompression rate for disequilibrium expansion is consistent with the estimated decompression rate for the explosive/effusive transition in natural basaltic eruptions.

Citation: Namiki, A., and M. Manga (2006), Influence of decompression rate on the expansion velocity and expansion style of bubbly fluids, *J. Geophys. Res.*, *111*, B11208, doi:10.1029/2005JB004132.

1. Introduction

[2] The decompression rate of magmas may be one of the key variables that influences whether ascending magma will erupt explosively. Estimated decompression rates for effusive and explosive eruptions typically differ by orders of magnitude [*Carey and Sigurdsson*, 1985; *Scandone and Malone*, 1985; *Rutherford and Hill*, 1993; *Geschwind and Rutherford*, 1995; *Nakada et al.*, 1995; *Kagiyama et al.*, 1999; *Rutherford and Gardner*, 2000; *Rutherford and Devine*, 2003], suggesting a connection between decompression rate and the fragmentation that accompanies explosive eruption [*Woods and Koyaguchi*, 1994; *Devine et al.*, 1998; *Martel and Schmidt*, 2003].

[3] The influence of decompression rate on bubble nucleation and growth has been studied experimentally [*Gardner et al.*, 1999; *Mangan and Sisson*, 2000; *Mourtada-Bonnefoi and Laporte*, 2004] and numerically [*Toramaru*, 1995; *Proussevitch and Sahagian*, 1996; *Yamada et al.*, 2005]. During fast decompression, volatile species are unable to exsolve fast enough, and the magma becomes supersaturated. The subsequent nucleation and growth of bubbles in a highly supersaturated melt can be a trigger for explosive eruption.

[4] *Ichihara et al.* [2002] address the importance of decompression rate for bubbly viscoelastic materials and show that slow decompression promotes nonexplosive expansion under conditions that would otherwise lead to fragmentation. Decompression rate is not, however, the only variable that determines the "style" of eruption and, in particular, whether magma can fragment. There is a critical pressure change needed in the limit of rapid decompression [e.g., *Alidibirov and Dingwell*, 1996]. The critical pressure change decreases if preexisting bubbles are present [e.g., *Martel et al.*, 2000], and the critical pressure change is found experimentally to depend inversely on initial vesicularity [*Spieler et al.*, 2004]. This scaling with vesicularity arises if the fragmentation threshold is governed by a critical enthalpy change that scales approximately with the product of pressure change and vesicularity [*Namiki and Manga*, 2005].

[5] It is often assumed that rapid decompression of bubbly magma causes explosive eruption, because bubbles are unable to expand sufficiently fast to allow the pressure inside bubbles to equilibrate with the pressure outside

[1]Department of Earth and Planetary Science, University of California Berkeley, Berkeley, California, USA.
[2]Now at Institute of Geology and Geoinformation, Magma Activity Research Group, Tsukuba, Japan.

0148-0227/06/2005JB004132$09.00

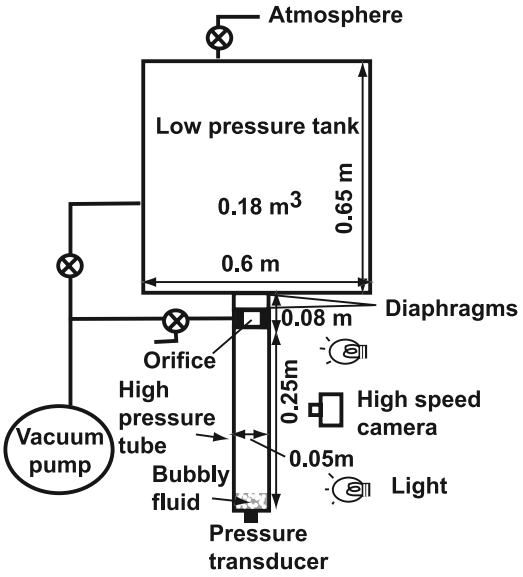

Figure 1. Illustration of the experimental apparatus.

bubbles. As a result, the pressure difference between the inside and outside of bubbles generates stress in the melt surrounding bubbles that can fragment the bubbly fluid in small pieces [*Zhang*, 1999; *Koyaguchi and Mitani*, 2005]. This explanation is appropriate for high-viscosity magmas in which the high viscosity of melt surrounding a bubble can retard bubble expansion. Numerical [e.g., *Thomas et al.*, 1994; *Barclay et al.*, 1995] and experimental [e.g., *Gardner et al.*, 2000; *Lensky et al.*, 2004] studies have shown that the required viscosity for such a viscous retardation depends on the decompression rate and that viscosities from 10^6 to 10^9 Pa s are required for realistic decompression rates.

[6] The mechanism through which low-viscosity magma can fragment and erupt explosively is less obvious. One mechanism that can lead to explosive eruptions is the interaction between magma and external water [e.g., *Sheridan and Wohletz*, 1983; *Mastin*, 1997]. Basaltic magma can also erupt explosively without any apparent role of external water during Hawaiian and Strombolian eruptions [e.g., *Vergniolle and Mangan*, 2000]. While basaltic Plinian eruptions are uncommon, they do occur [e.g., *Walker et al.*, 1984]. *Houghton et al.* [2004] suggest that rapid ascent at conduit constrictions can sustain basaltic Plinian eruptions.

[7] In the present paper we conduct a series of decompression experiments with bubbly fluids for a range of decompression rates. We propose a mechanism that generates a pressure difference between the inside and outside of bubbles without viscous retardation of bubble growth.

2. Experimental Procedure

[8] We conduct decompression experiments in the shock tube-type apparatus illustrated in Figure 1. This is a widely used method to simulate the rapid decompression of analogue magmatic materials [e.g., *Mader*, 1998]. The bubbly fluid is contained in the high-pressure shock tube and is separated from a large low-pressure tank by diaphragms. The diaphragms are made of either commercial aluminum foil or 2–10 μm thick polyester films. When the diaphragms break, a rarefaction wave propagates into the tube and the bubbly fluid experiences decompression. The shock tube has an inner diameter of 0.05 m and a length of 0.25 m. The volume of the low-pressure tank is 0.18 m^3. The initial pressure in the shock tube P_{Gi} is atmospheric pressure (10^5 Pa), and pressure inside the low-pressure tank P_{Of} is variable. We use subscripts G, O, i, and f to denote gas inside bubbles, outside bubbles, and initial and final states, respectively. Notation is summarized in Table 1. For our magma analogue, we use xanthan gum solutions. To stabilize bubbles we add 0.4 vol % hand soap, which acts as a surfactant. Bubbles are added by a hand mixer. The physical properties of this bubbly fluid are reported by *Namiki and Manga* [2005].

Table 1. Notation

Parameter	Description	Unit
ϕ	vesicularity (volume fraction of bubbles)	
$\dot{\epsilon}$	shear rate	s^{-1}
γ	isentropic exponent	
ρ	density	kg m^{-3}
η	viscosity for bubble-free liquid	Pa s
σ	surface tension	N m^{-1}
$\Delta\hat{H}_{mod}$	volumetric enthalpy change by decompression, equation (6)	J m^{-3}
A	cross section area of exit flow	m^2
A_h	cross section area of the high-pressure tube	m^2
C	semimajor axis length of bubble	m
c_0	sound velocity of air	m s^{-1}
g	gravitational acceleration	m s^{-2}
h	height of a bubbly fluid column	m
L	diameter of high-pressure tube	m
P	pressure	Pa
ΔP	$P_{Gi}-P_{Of}$	Pa
R	bubble radius	m
Re_b	Reynolds number for bubble film, equation (14)	
Re_c	Reynolds number for bubbly fluid column, equation (12)	
R_{ori}	ratio of the high-pressure tube radius to the orifice radius	
t	time	s
t_p	time when decompression ends	s
V	volume	m^3
V_h	volume of high-pressure tube	m^3
v_d	disequilibrium expansion velocity of bubbly fluid, equation (5)	m s^{-1}
v_{dT}	disequilibrium expansion velocity for constant temperature, equation (9)	m s^{-1}
v_e	equilibrium expansion velocity of bubbly fluid, equation (4)	m s^{-1}
v_m	measured expansion velocity of bubbly fluid	m s^{-1}
	Subscripts	
G	gas inside bubbles	
O	gas outside bubbles	
F	bubbly fluid	
L	liquid	
M	magma	
i	initial $t \leq 0$	
t	during decompression, $0 < t < t_p$	
f	final $t \geq t_p$	

Table 2. Experimental Conditions and Results

R_{ori}	ϕ_i	P_{Gi}, 10^5 Pa	P_{Of}, 10^5 Pa	ΔP, 10^5 Pa	h_{Fi}, m	t_p, s	Type
			Set 1				
1	0.60	0.91	0.11	0.81	0.035	0.003	fragmentation
1/2	0.64	0.98	0.14	0.84	0.040	0.010	fragmentation
1/4	0.63	1.00	0.12	0.88	0.048	0.045	expansion
1/8	0.63	1.00	0.18	0.83	0.050	0.145	expansion
1/16	0.62	1.03	0.18	0.85	0.050	0.579	expansion
			Set 2				
1	0.69	0.90	0.24	0.66	0.041	0.002	fragmentation
1/2	0.61	1.00	0.33	0.67	0.049	0.006	fragmentation
1/4	0.62	1.02	0.35	0.67	0.050	0.021	expansion
1/8	0.65	1.01	0.34	0.66	0.048	0.085	expansion
1/16	0.62	1.00	0.35	0.65	0.044	0.332	expansion
			Set 3				
1	0.22	1.01	0.07	0.94	0.051	0.004	fragmentation
1/2	0.25	0.99	0.06	0.94	0.040	0.016	fragmentation
1/4	0.19	1.00	0.08	0.92	0.041	0.056	expansion
1/8	0.26	1.01	0.10	0.91	0.058	0.201	expansion
1/16	0.20	1.01	0.08	0.93	0.043	0.891	expansion
			Set 4				
1	0.79	1.00	0.60	0.41	0.050	0.001	partial rupture
1/2	0.82	1.00	0.58	0.42	0.028	0.003	partial rupture
1/4	0.80	0.99	0.53	0.46	0.034	0.012	expansion
1/8	0.76	1.00	0.52	0.48	0.044	0.050	expansion
1/16	0.82	0.99	0.53	0.47	0.041	0.194	expansion
			Set 5				
1	0.23	1.01	0.35	0.66	0.031	0.001	detachment
1/2	0.22	1.00	0.34	0.66	0.043	0.005	detachment
1/4	0.22	1.01	0.34	0.67	0.043	0.021	expansion
1/8	0.27	1.00	0.33	0.67	0.041	0.087	expansion
1/16	0.24	1.00	0.34	0.66	0.040	0.343	expansion

[9] The decompression rate is varied by changing the orifice diameter. Larger orifice diameters permit faster decompressions. This is the same technique used by *Ichihara et al.* [2002]. The orifice is located between the diaphragm and the high-pressure tube so that the diameter of the high-pressure tube is uniform for all decompression rates. We describe and characterize phenomena in the high-pressure tube only below the orifice.

[10] We use five different orifices. The ratios of those diameters to the shock tube diameter $L = 0.05$ m are $R_{ori} = 1$, 1/2, 1/4,1/8, and 1/16 where $R_{ori} = 1$ provides the highest decompression rate and lower values provide lower decompression rates. Pressure in the tube is measured with a pressure transducer whose response time is 2 ms, and is recorded by a digital oscilloscope. In the appendix, the decompression rate as a function of orifice size is derived and compared with measurements. The response of bubbly fluid is recorded by a high-speed digital camera with a maximum frame rate of 2000 frames per second with resolution of 256 $\times$ 1280 pixels.

[11] We conduct five sets of experiments; each set consists of five experiments with different decompression rates R_{ori} = 1,1/2, 1/4, 1/8, and 1/16 at similar initial vesicularity ϕ_i and pressure difference between two tanks $\Delta P = P_{Gi} - P_{Of}$. Initial vesicularity ϕ_i and pressure difference ΔP for the five sets are listed in Table 2.

[12] In our previous experiments based on rapid decompression $R_{ori} = 1$, we found several regimes of expansion style by varying the initial vesicularity and pressure difference. Three styles of eruptions are relevant for the present study; ''fragmentation,'' ''partial rupture,'' and ''detachment.'' In the detachment regime, decompressed bubbly fluid elongates vertically, shrinks radially, and detaches from the high-pressure tube wall. In the partial rupture regime, in addition to vertical elongation of the fluid, several large voids develop within the fluid. This suggests that the bubble walls rupture and bubbles become interconnected. In this case, walls rupture but plateau borders remain connected. In contrast to the detachment case, the fluid does not shrink radially. In the fragmentation regime, in addition to phenomena observed in the partial rupture regime, the bubbly fluid fragments layer-by-layer and erupts discrete parcels of fluid. In the present paper, we use the term fragmentation exclusively for the case in which fluid parcels are generated.

[13] In the study reported here, three of five experimental sets are conducted with vesicularities and pressure differences for the fragmentation regime in rapid decompression ($R_{ori} = 1$). The other two sets of experiments are conducted for conditions that lead to partial rupture and detachment during rapid decompression.

3. Results

[14] Figures 2–4 show the range of phenomena seen in our experiments. In general, when the decompression rate is higher ($R_{ori} \geq 1/2$), a variety of expansion styles can result,

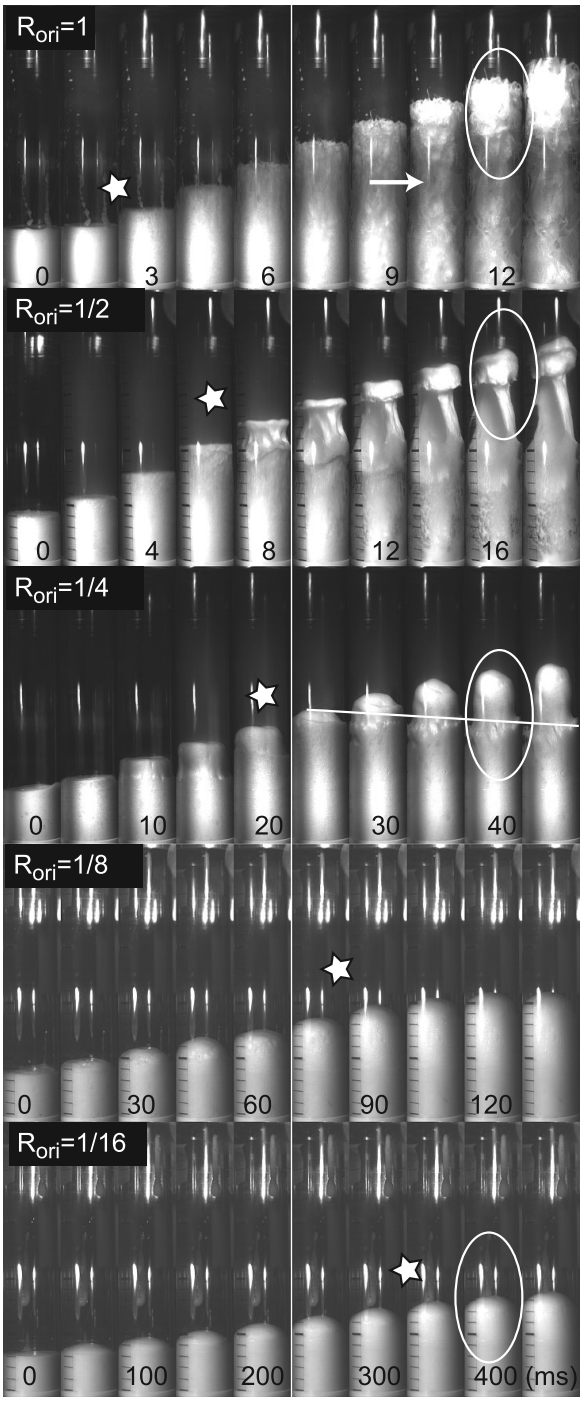

Figure 2. Digital photographs showing the response of the bubbly fluid in the shock tube for experimental set 2. Each column shows a snapshot of the high-pressure tube whose height is 0.25 m and diameter is 0.05 m. The brightness of the fluid depends on vesicularity. Each column shows five different experiments with R_{ori} = 1, 1/2, 1/4, 1/8, and 1/16, respectively. Numbers at the bottom of each snapshot show the elapsed time in milliseconds. Stars show the estimated time when decompression ends, given by equation (A3). A movie of this figure is provided as Animation 1 in the auxiliary material.

including fragmentation, depending on ϕ_i and ΔP. When the decompression rate is lower ($R_{ori} \leq 1/4$), however, the bubbly fluid only expands. The threshold decompression rate that limits the response to expansion in the present experiments is associated with $R_{ori} = 1/2$.

3.1. Visual Observations in Fragmentation Regime

[15] Figure 2 shows the results of experimental set 2 in which $\phi_i \sim 0.6$ and $\Delta P \sim 6 \times 10^4$ Pa (see Animation 1 in the auxiliary material for a movie of Figure 2).[1] The most obvious difference between these five experiments with different decompression rates is the timescale over which the bubbly fluid expands. For the larger R_{ori} which provide higher decompression rates, the bubbly fluid expands faster.

[16] The expansion style also differs among these experiments. For the experiment with $R_{ori} = 1$, the flow front of the bubbly fluid develops a rough surface, suggesting the rupture of liquid films between bubbles (indicated by the white circle). The side view shows some black spots, which are voids made following the coalescence of bubbles after rupture of the liquid films separating bubbles. The bubbly fluid fragments in two parts, breaking near the middle of the fluid column (indicated by the white arrow). The expanding fluid is ejected into the low-pressure tank and hits the tank's roof. These features describe the regime we term fragmentation.

[17] The experiment with $R_{ori} = 1/2$ also shows the separation of the top and bottom parts of the expanding fluid (indicated by the white circle). Different from the experiment with $R_{ori} = 1$, a rough surface does not develop on the top of the expanding fluid, suggesting that the films separating bubbles are not rupturing.

[18] In the experiment with $R_{ori} = 1/4$, fragmentation is not observed. Accompanying the decompression, the central part of the bubbly fluid first expands without maintaining contact with the tube wall. At 20 ms, the bubbly fluid in contact with tube wall begins to expand. After 30 ms, the bubbly fluid at the center of the tube continues to expand but the fluid contacting the tube wall retracts, as indicated by the sloping white line. Except for the largest bubbles with diameters of several millimeters, bubbles maintain their spherical shapes during expansion.

[19] In experiments with $R_{ori} = 1/8$ and 1/16, fragmentation and detachment are not observed. The bubbly fluid always remains in contact with the tube wall. The top of the bubbly fluid has a convex shape. Bubbles remain spherical. The final height of bubbly fluid is much lower than that observed for larger R_{ori}. We refer to this style of expansion as "expansion."

[20] In experiments with $R_{ori} = 1/8$ and 1/16, expansion stops at almost the same time as the end of decompression indicated with stars in Figures 2–4. In experiments with $R_{ori} = 1$, 1/2, and 1/4, however, expansion continues after the decompression ends. Fragmentation and detachment occur after the decompression ends.

[21] Observed features in experimental sets 1 and 3 are similar to those observed in set 2. The expansion of bubbly fluid with larger R_{ori} is faster. The experiments with $R_{ori} = 1$ have a rough flow front and the bubbly fluid fragments. The

[1] Auxiliary materials are available in the HTML. doi:10.1029/2005JB004132.

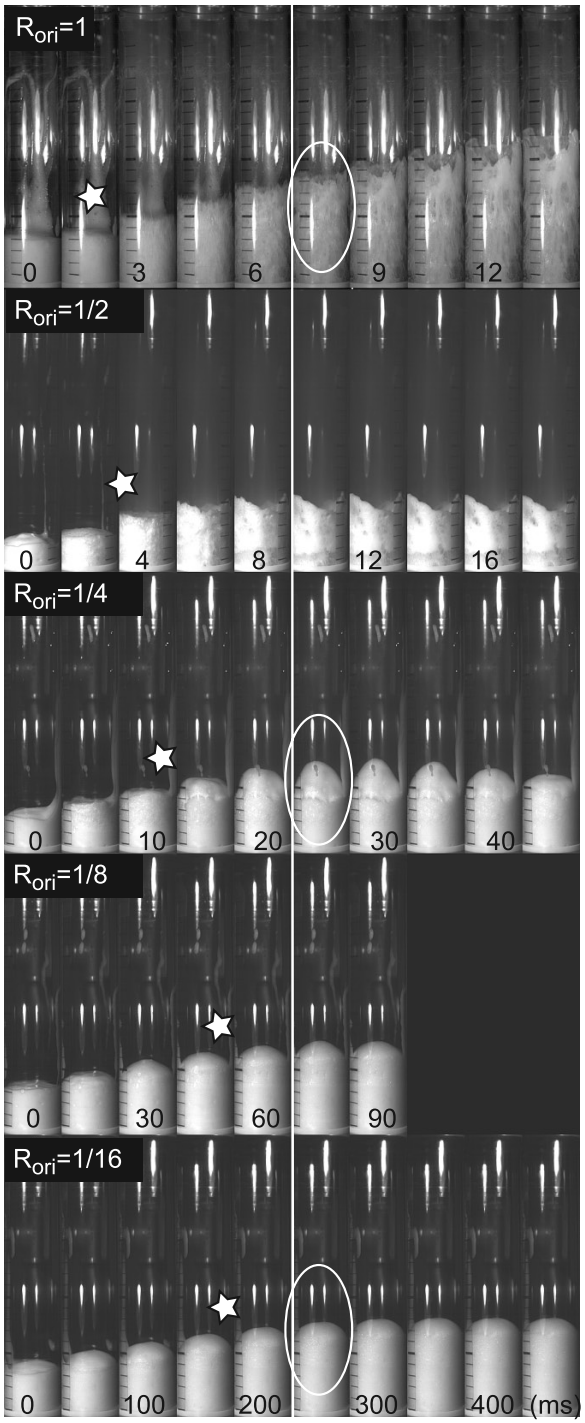

Figure 3. Same as Figure 2 but for set 4.

rough upper surface is not apparent for R_{ori} = 1/2. For the experiment with R_{ori} = 1/4 in set 3, detachment is observed. In set 1, the fluid expands while in contact with tube wall until it reaches the end of the tube, so detachment cannot be observed. Experiments with R_{ori} = 1/8 and 1/16 show expansion. In sets 1 and 3, the expansion of bubbly fluid continues after the decompression ends in all experiments.

3.2. Visual Observations in Partial Rupture Regime

[22] Figure 3 shows the results of experimental set 4 with $\phi_i \sim 0.8$ and $\Delta P \sim 4 \times 10^4$ Pa. The experiment with R_{ori} = 1 shows a texture that resembles a net. It develops following the rupture of films separating bubbles, indicated by the white circle. This pattern is classified as partial rupture. The experiment with R_{ori} = 1/2 shows similar patterns; however, the fluid adheres to the tube and the expansion stops by 8 ms. In the experiment with R_{ori} = 1/4, the bubbly fluid continues to expand until 30 ms and develops a cone shape, as indicated by the white circle. The flow front then retracts and becomes flat. Experiments with R_{ori} = 1/8 and 1/16 show expansion, where the flow front has a convex shape and the bubbles maintain spherical shapes, indicated by the

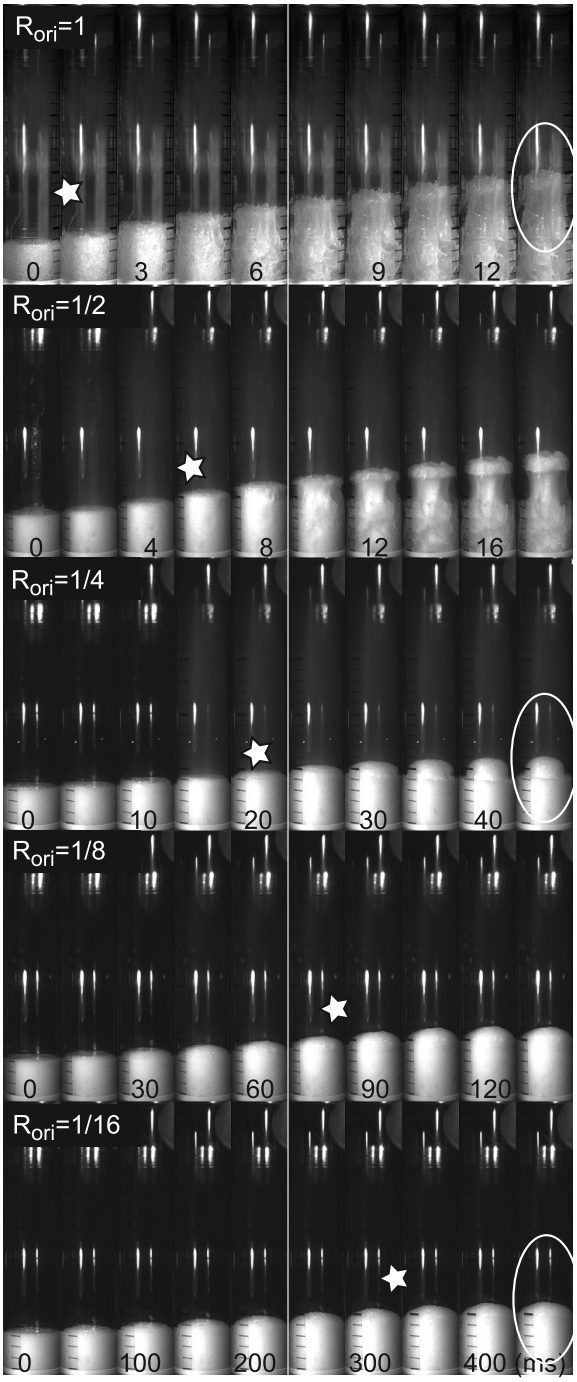

Figure 4. Same as Figure 2 but for set 5.

white circle. In these two experiments, expansion ends when the decompression ends.

3.3. Visual Observations in Detachment Regime

[23] Figure 4 shows the results of experimental set 5 with $\phi_i \sim 0.2$ and $\Delta P \sim 6 \times 10^4$ Pa. In experiments with $R_{ori} = 1$ and 1/2, the bubbly fluid elongates vertically and detaches from the tube wall, a response termed detachment. Detachment is observed after the decompression ends. Also, in the experiment with $R_{ori} = 1/4$, the center of the bubbly fluid detaches from the tube wall after the decompression ends, although its shape is different from experiments with $R_{ori} \geq 1/2$, as indicated by the white circles. Experiments $R_{ori} = 1/8$ and 1/16 show expansion with a convex flow front, indicated by the white circle.

4. Discussion

[24] Our experimental results clearly show the importance of the decompression rate on the expansion style and velocity, and we find that there is a critical decompression rate at which the expansion style changes. To explain the effect of decompression rate on transitions in eruption style, we introduce and compare two important velocities: equilibrium expansion velocity v_e and disequilibrium expansion velocity v_d.

[25] The gas inside bubbles cannot expand instantaneously in response to pressure changes. There is an upper limit velocity v_d of the expansion velocity. If the decompression is sufficiently fast, the expansion velocity v_e required for bubbles to immediately adjust to the pressure change is greater than this upper bound (i.e., $v_e > v_d$), and v_d will limit the expansion. In this case, the gas pressure inside the bubbles will not be equal to the pressure outside the bubbles, and we term this case "disequilibrium" expansion. In contrast, if the decompression is slow enough (i.e., $v_e < v_d$), the pressure inside the bubbles remains in "equilibrium" with the pressure outside the bubbles. We hypothesize that fragmentation and partial rupture requires $v_e > v_d$, in addition to sufficiently large changes in enthalpy which is a function of the initial and final pressures P_{Gi}, P_{Of} and initial vesicularity ϕ_i, as found in previous studies [e.g., *Spieler et al.*, 2004; *Namiki and Manga*, 2005]. To test our hypothesis, we compare the height change of the bubbly fluid caused by disequilibrium and equilibrium expansion with the measured height change.

4.1. Theoretical Estimate of Expansion Velocities

4.1.1. Equilibrium Expansion

[26] Here we estimate the volume change of bubbly fluid when the pressures inside P_{Gt} and outside P_{Ot} bubbles are equal. The subscript t indicates a time during the decompression $0 < t < t_p$. We neglect the effect of surface tension.

[27] The transient volume of bubbly fluid V_{Ft} is the sum of the volume of gas V_{Gt} and the volume of liquid V_{Lt},

$$V_{Ft} = V_{Gt} + V_{Lt}, \tag{1}$$

where the subscript F indicates values for the bubbly fluid. We assume that, under sufficiently slow decompression, the heat is transferred between the expanding gas and the surrounding liquid such that the gas inside bubbles remains isothermal. The ideal gas law then implies that $V_{Gt} = (P_{Gi}/P_{Ot})\, V_{Gi}$. The transient volume of the bubbly fluid for isothermal expansion is thus

$$V_{Ft} = \left(\frac{P_{Gi}}{P_{Ot}}\right) V_{Gi} + V_{Li}, \tag{2}$$

where we neglect the volume change of the liquid phase because it is so much less compressible than gas (i.e., $V_{Li} = V_{Lt}$). Dividing both sides of equation (2) by the initial bubbly fluid volume V_{Fi}, and assuming that the cross section area of the expanding column of fluid is constant, we obtain an equation for the height of the bubbly fluid column h,

$$\frac{h_{Ft}}{h_{Fi}} = \left(\frac{P_{Gi}}{P_{Ot}}\right) \phi_i + 1 - \phi_i. \tag{3}$$

From equation (3) we can obtain the height change of the equilibrium flow front $h_{Ft} - h_{Fi}$.

[28] The predicted equilibrium expansion is shown in Figure 5 with red curves, where the transient pressure P_{Ot} is obtained from equation (A1). After the outside pressure reaches the final pressure, $P_{Ot} = P_{Of}$, the height is assumed to remain constant. The time when the height reaches a constant is the time when decompression ends, t_p.

[29] The equilibrium expansion velocity is given by the time derivative of equation (3)

$$v_e = \frac{dh_{Ft}}{dt} = -\frac{\phi_i h_{Fi} P_{Gi}}{P_{Ot}^2} \dot{P}_{Ot}, \tag{4}$$

where the time derivative of pressure $\dot{P}_{Ot}$ is calculated from equation (A4).

4.1.2. Disequilibrium Expansion

[30] *Namiki and Manga* [2005] estimate the expansion velocity assuming that the volumetric enthalpy change caused by an instantaneous pressure change is transformed to kinetic energy. Here we modify the model to include the effect of time-varying pressure, that is,

$$v_d = \sqrt{\frac{2}{\rho_{Fi}} \Delta \hat{H}_{mod}}, \tag{5}$$

with

$$\Delta \hat{H}_{mod} = \frac{\gamma P_{Gi} \phi_i}{\gamma - 1} \left\{ 1 - \left(\frac{P_{Ot}}{P_{Gi}}\right)^{\frac{\gamma-1}{\gamma}} \right\} - \phi_i P_{Of} \left\{ \left(\frac{P_{Gi}}{P_{Ot}}\right)^{1/\gamma} - 1 \right\}, \tag{6}$$

where ρ_F is density of the bubbly fluid and γ is the isentropic exponent. $\Delta \hat{H}_{mod}$ is the modified volumetric enthalpy change, and first term is the enthalpy change due to decompression and the second term is the required work to compress the gas in the low-pressure tank. The second term should not be important in real volcanic eruptions, because the atmosphere, represented by the low-pressure tank, has, effectively, infinite volume. Here, the transient pressure P_{Ot} is the outside pressure during the decompression, $0 < t < t_p$, and is estimated by equation (A1). After the

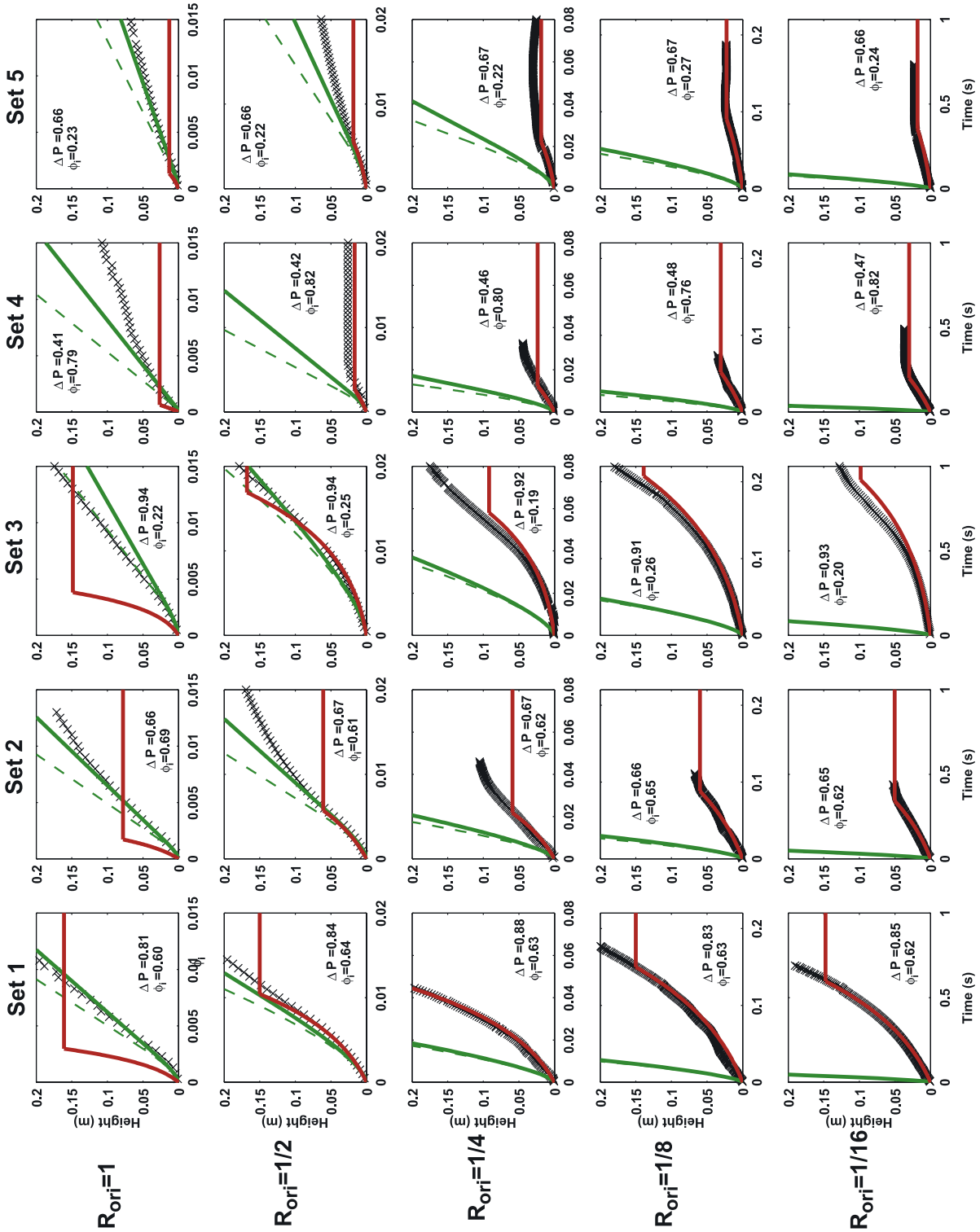

Figure 5. Flow front height as a function of time for each experiment. Black crosses show measured height. Solid and dashed green curves show the calculated height, given by equations (5), (7) and (9) for disequilibrium without and with heat exchange between gas inside bubbles and surrounding liquid, respectively. Red curve shows the calculated height by equation (3) for equilibrium expansion.

decompression ends, $t \geq t_p$, the outside pressure is assumed to be identical to the final outside pressure $P_{Ot} = P_{Of}$, so that the expansion velocity becomes the same as that when the decompression ends. These equations imply that the pressure change is immediately reflected in the velocity, and the velocity represents the integrated enthalpy change during the decompression. This equation is applicable when the deceleration terms due viscosity and gravity can be neglected, so that the enthalpy change immediately changes the kinetic energy.

[31] Using the expansion velocity v_d, the height change of the disequilibrium flow front $h_{Ft} - h_{Fi}$ is obtained by integrating over time,

$$h_{Ft} - h_{Fi} = \int_0^t v_d \, dt'. \tag{7}$$

This estimate is shown by solid green curves in Figure 5.

[32] In our derivation of equation (5), heat exchange between bubbles and the surrounding liquid is not included. When the vesicularity is small and expansion velocity is slow, heat exchange cannot be neglected. When heat exchange is important, we use a formulation for constant temperature expansion. The energy which can be used to expand the gas at constant temperature is given by

$$\Delta\hat{Q} = \frac{\phi_i}{V_{Gi}} \int_{V_{Gi}}^{V_{Gt}} P \, dV. \tag{8}$$

Here we use $V_{Gi}P_{Gi} = PV$. If this energy is transferred to kinetic energy, the expansion velocity v_{dT} becomes

$$v_{dT} = \left(\frac{2\phi_i \Delta\hat{Q}}{\rho_{Fi}}\right)^{1/2} = \left\{\frac{2P_{Gi}\phi_i}{\rho_{Fi}} \ln\left(\frac{P_{Gi}}{P_{Gt}}\right)\right\}^{1/2}. \tag{9}$$

The height change of the flow front is calculated by integrating v_{dT} in the same manner as in equation (7). This estimate is shown by a dashed green curve in Figure 5.

[33] Both of the solid and dashed green curves indicate disequilibrium expansion. The difference between these two curves is whether the gas inside bubbles expands without or with heat exchange to the surrounding liquid, respectively. Similar formulations are derived by *Self et al.* [1979] and *Mastin* [1995].

4.1.3. Comparison With Measured Height

[34] In Figure 5, we compare the observed flow front heights for the equilibrium and disequilibrium models. Calculated equilibrium expansion (red curves) is faster than disequilibrium expansion (solid and dashed green curves) for decompression rates associated with $R_{ori} > 1/2$, but disequilibrium expansion becomes faster when decompression is slower ($R_{ori} \leq 1/4$). This result suggests that the threshold $v_e \approx v_d$ occurs around $R_{ori} \approx 1/2$.

[35] Figure 5 for $R_{ori} \geq 1/2$, shows that the initial flow front velocity follows the disequilibrium estimate (solid or dashed green curves). Most of these cases follow solid green curves, implying adiabatic expansion, by equation (5), and negligible heat exchange between the gas inside bubbles and the surrounding liquid. For $R_{ori} = 1$ and experimental set 3, however, the observed flow front velocity is faster than the adiabatic estimate. The expansion velocity at constant temperature (equation (9)) explains the measured flow front position. We interpret this to indicate that some heat exchange occurs between the gas and surrounding liquid and that this energy transfer accelerates the expansion. This may be because the initial vesicularity is small, $\phi_i = 0.22$. In most cases, heat exchange between the gas inside bubbles and surrounding liquid is not significant, so we use the adiabatic estimate v_d as a representative velocity for disequilibrium expansion in the rest of this discussion.

[36] In experimental sets 2, 4, and 5, the flow front decelerates after the decompression ends. In these experiments, because the fluid does not fragment or does not fragment completely, viscous stresses act to decelerate the fluid. For $R_{ori} = 1/2$ and experimental set 4, the expansion ends at 0.005 s. This is because the expanding fluid adheres to the tube wall, a process that is not modeled.

[37] In experiments with $R_{ori} = 1/4$, 1/8, and 1/16, the flow front position is well explained by the equilibrium expansion estimate (red curves). Experiments with $R_{ori} = 1/4$ show that the final height of the bubbly fluid exceeds the estimated one by equilibrium expansion, except in set 1 where the estimated final height is above the tube height. In experiments with $R_{ori} = 1/8$ and 1/16, the final heights of experimental sets 2, 4, and 5 are well explained by equilibrium expansion. However, the final heights in experimental sets 1 and 3 exceed the estimated height.

[38] These results indicate that there is an upper limit for the velocity of bubble expansion. When decompression is faster than this upper limit, the bubble expansion velocity follows the upper limit, the disequilibrium expansion velocity. However, when decompression is sufficiently slow, the bubble expansion velocity follows equilibrium expansion.

4.2. Interpretation of Visual Observations

4.2.1. Fragmentation and Rupture of Bubble Films

[39] In our visual observations, we find that the fragmentation of bubbly fluid requires at least $R_{ori} \geq 1/2$. The rupture of films between bubbles is apparent mainly for $R_{ori} = 1$. At the decompression rates corresponding to $R_{ori} > 1/2$, the measured flow front heights reflect disequilibrium expansion. As a consequence, we infer that the pressure difference between the inside and outside of bubbles provides the driving force that ruptures the film between bubbles.

[40] To confirm this hypothesis, we calculate the pressure inside bubbles from the measured flow front position h_{Ft}, using the equation of state for an ideal gas,

$$P_{Gt}h_{Ft}\phi_t = P_{Gi}h_{Gi}\phi_i, \tag{10}$$

where ϕ_t is calculated assuming the liquid is incompressible and the cross section of the fluid column remains constant:

$$h_{Ft}(1 - \phi_t) = h_{Fi}(1 - \phi_i). \tag{11}$$

Equations (10) and hence (11) include the approximation that temperature remains constant, even though in many cases the expansion is adiabatic and a temperature reduction is expected.

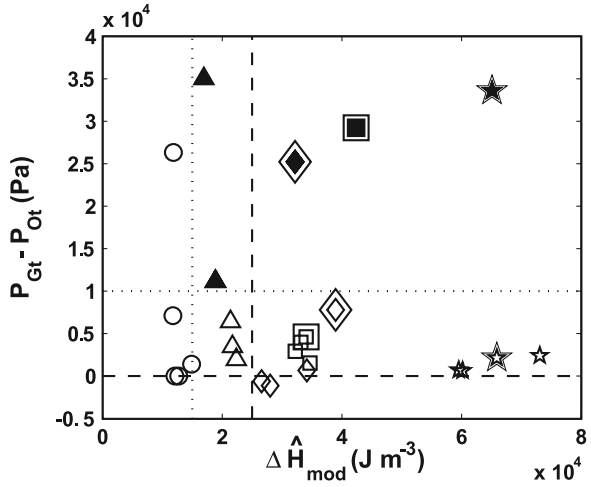

Figure 6. Maximum pressure difference between the inside and outside of bubbles, calculated from the measured flow front position and equation (A1), as a function of volumetric enthalpy change $\Delta\hat{H}_{\mathrm{mod}}$. The star, square, diamond, triangle, and circle indicate sets 1 through 5, respectively. Solid symbols indicate that partial rupture is observed; ringed symbols indicate that fragmentation is observed.

[41] Figure 6 shows the calculated maximum pressure difference between the inside and outside of the bubbles during the decompression, $P_{\mathrm{Gt}}-P_{\mathrm{Ot}}$, as a function of the enthalpy change $\Delta\hat{H}_{\mathrm{mod}}$. Ringed symbols indicate experiments in which fragmentation is observed, and solid symbols indicate experiments in which we observe the rupture of bubble films. Figure 6 shows that partial rupture requires a critical pressure difference $>10^4$ Pa between the inside and outside of the bubbles (denoted by a dotted line). A constant enthalpy change 1.5×10^4 J m^{-3} also apparently separates experiments that result in partial rupture from those in which no rupture is observed.

[42] Figure 6 shows that the importance of the pressure difference is difficult to assess for fragmentation. Figure 6 only shows that fragmentation requires a positive pressure difference and a sufficiently large enthalpy change (2.5×10^4 J m^{-3} denoted by dashed lines). However, the difference of the calculated overpressure $P_{\mathrm{Gt}}-P_{\mathrm{Ot}}$ between the experiments with $R_{\mathrm{ori}} = 1/2$ (fragmentation case) and $R_{\mathrm{ori}} \leq 1/4$ (expansion cases) is not significant. We thus hypothesize that the appropriate threshold for fragmentation is $v_{\mathrm{e}} \geq v_{\mathrm{d}}$, as we discussed in Figure 5.

[43] During disequilibrium expansion, the fluid does not expand homogeneously. The top part expands first, and the bottom part expands after a delay. From these observations, we can thus also infer that the criterion $v_{\mathrm{e}} \geq v_{\mathrm{d}}$ indicates whether the entire fluid column can expand homogeneously. Localized vertical strain caused by inhomogeneous expansion generates additional stresses that may promote fragmentation even when the overpressure $P_{\mathrm{Gt}}-P_{\mathrm{Ot}}$ is negligible. This hypothesis implies that fragmentation behavior is closely related to the propagation of the decompression wave, as pointed out by *Koyaguchi and Mitani* [2005] and *Toramaru* [2006].

[44] We note that the calculated pressure difference is sensitive to when we identify the initiation of decompression (time $t = 0$). In our apparatus, we cannot measure $t = 0$, and we use the time when the bubbly fluid begins expansion from the visual observation in the high speed video as $t = 0$. This might introduce some error in the calculated pressure difference.

[45] In summary, we interpret our results to indicate that a requirement for fragmentation is $v_{\mathrm{e}} \geq v_{\mathrm{d}}$ and that for partial rupture is $v_{\mathrm{e}} - v_{\mathrm{d}} >$ some constant value, to generate overpressure.

4.2.2. Detachment

[46] In experiments with $R_{\mathrm{ori}} \leq 1/4$, the measured flow front height follows the equilibrium expansion estimate (Figure 5). The measured final height, however, sometimes exceeds the estimated height by equilibrium expansion. In our visual observations, we find that detachment occurs after the decompression ends. The bubbly fluid is in contact with the tube wall which provides a no-slip boundary condition and leads to the convex flow front. After the decompression ends, the width of the fluid column decreases as the bubbly fluid detaches from the tube wall (Figure 2; $R_{\mathrm{ori}} = 1/4$), then the flow front retracts (Figure 3; $R_{\mathrm{ori}} = 1/4$). These features suggest that the flow front is overshooting an equilibrium position.

[47] To explain the occurrence of overshoot, we calculate the Reynolds number (the relative importance of inertial and viscous forces) for the fluid column:

$$\mathrm{Re}_{\mathrm{c}} = \frac{\rho_{\mathrm{Ft}} v_{\mathrm{m}} L}{\eta}, \tag{12}$$

where we use the measured front velocity as v_{m} and use the diameter of tube 0.05 m for length scale L. Viscosity η is obtained from the measured shear rate dependence from

$$\eta = 5.7\dot{\epsilon}^{-0.73}, \tag{13}$$

a relationship we determined experimentally [*Namiki and Manga*, 2005]. The shear rate is calculated from $\dot{\epsilon} = v_{\mathrm{m}}/h_{\mathrm{Ft}}$.

[48] Figure 7a shows the calculated Re_{c}. Solid symbols indicate experiments in which the measured final height exceeds the predicted one by equilibrium expansion. Except for two experiments with $R_{\mathrm{ori}} = 1/16$ in sets 1 and 3, a constant $\mathrm{Re}_{\mathrm{c}} \approx 5$ separates the solid and open symbols. In these two anomalous experiments, the final pressure is close to the saturation pressure of water. If the surrounding temperature is higher than the room temperature, some of the liquid in the bubbly fluid will evaporate and the bubbles will expand still further. The lights used to illuminate the bubbly fluid do increase the temperature locally. We thus interpret the data in Figure 7a to show that overshoot is driven by the inertia of the expanding fluid because it occurs when $\mathrm{Re}_{\mathrm{c}} \gg 1$.

[49] The measured height in experiments with $R_{\mathrm{ori}} \leq 1/4$ follows equilibrium expansion throughout the decompression, indicating that there is no overshoot until the decompression ends. To understand why, we calculate the Reynolds number characterizing the flow in bubble films,

$$\mathrm{Re}_{\mathrm{b}} = \frac{\rho_{\mathrm{l}} \dot{R}_{\mathrm{t}} R_{\mathrm{t}}}{\eta}, \tag{14}$$

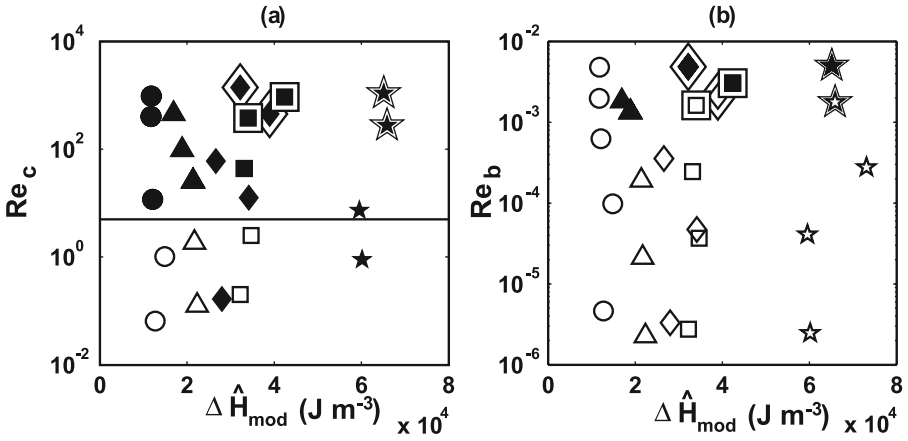

Figure 7. (a) Calculated Reynolds number for the fluid column when decompression ends at $t = t_p$, calculated from equation (12). Symbols used are the same as those in Figure 6, except for the solid symbol which indicates that the measured final height exceeds that estimated by equilibrium expansion. Experimental set 1 for $R_{ori} = 1/4$ is not plotted here. (b) Maximum Reynolds number for flow of liquid in bubble films calculated from equation (14). Symbols used are the same as those used in Figure 7a, but solid symbols indicate that rupture of bubble films is observed.

where R is the bubble radius and the dot is used to indicate a time derivative. Bubble radius during the decompression R_t is calculated with the assumption that bubble expansion governs the volume change

$$\left(\frac{R_t}{R_i}\right)^3 = \frac{h_{Ft}\phi_t}{h_{Fi}\phi_i}, \tag{15}$$

where the time-dependent vesicularity ϕ_t is calculated from equation (11). For the initial bubble radius, we use an averaged value for our experiments $R_i = 63$ μm. The expansion velocity for each bubble $\dot{R}_t$ is calculated from the derivative of equation (15),

$$\dot{R}_t = \frac{R_i}{3h_{Fi}\phi_i}\left(1 - \frac{1}{\phi_i} + \frac{h_{Ft}}{h_{Fi}\phi_i}\right)^{-2/3} v_m. \tag{16}$$

Viscosity is calculated from equation (13), where the shear rate is calculated by $\dot{\epsilon} = \dot{R}_t/R_t$.

[50] Figure 7b shows the calculated maximum Reynolds number for the flow in bubble films and indicates that $Re_b \ll 1$ for all experiments regardless of the expansion style. Inertia thus plays no significant role in the expansion of bubbles, only (in some cases) for the dynamics of the fluid column as a whole.

[51] Hence when the Reynolds number for whole fluid column exceeds $Re_c \gg 1$, the flow front cannot stop when the decompression ends, even if the pressure inside bubbles is already equal to that outside bubbles. In this situation, bubbles do not expand, and the bubbly fluid elongates vertically while maintaining a constant volume. The fluid must thus detach from the tube wall. From these results, we infer that the expansion style we classify as detachment is a result of inertia-driven overshoot.

4.2.3. Deformation of Bubbles

[52] Deformation of bubbles is frequently discussed because of the importance of bubble connectivity on gas permeability of bubbly magma [*Klug and Cashman*, 1996; *Saar and Manga*, 1999; *Larsen et al.*, 2004; *Burgisser and Gardner*, 2005; *Gaonac'h et al.*, 2005]. In our visual observations, deformation of bubbles is observed only during fast decompression. To understand the relationship between the vertical expansion of whole fluid column and the deformation of each bubble, we calculate the Capillary number, which is a ratio of viscous stresses, which act to deform bubbles, and surface tension stresses, which act to keep bubbles spherical,

$$\mathrm{Ca} = \frac{\eta\dot{\epsilon}R_i}{\sigma}. \tag{17}$$

We use a surface tension $\sigma = 35$ mN m^{-1}, a value for water saturated with surfactant [*Hamley*, 2000]. The shear rate $\dot{\epsilon}$ is calculated assuming that bubbles elongate vertically while maintaining a spheroidal shape. The semiminor axis length thus becomes R_i, and the relation between the semimajor axis length C_t and the flow front height change can be calculated from

$$\frac{4\pi R_i^2 C_t/3}{4\pi R_i^3/3} = \frac{h_{Ft}\phi_t}{h_{Fi}\phi_i}, \tag{18}$$

where the transient vesicularity ϕ_t is calculated from equation (11). The shear rate is obtained from

$$\dot{\epsilon} = \frac{\dot{C}_t}{R_i} = \frac{v_m}{h_{Fi}\phi_i}. \tag{19}$$

We calculate viscosity η, using equation (13) with this shear rate.

[53] Figure 8a shows the calculated Capillary numbers using the average initial bubble radius of 63 μm. Experiments resulting in fragmentation are shown with ringed symbols, and those in which partial rupture is observed are shown with solid symbols. We note that in all experiments, the Capillary number for the average initial bubble radius does not exceed 1, a limit above which deformation will be significant and readily observed. The correlation between

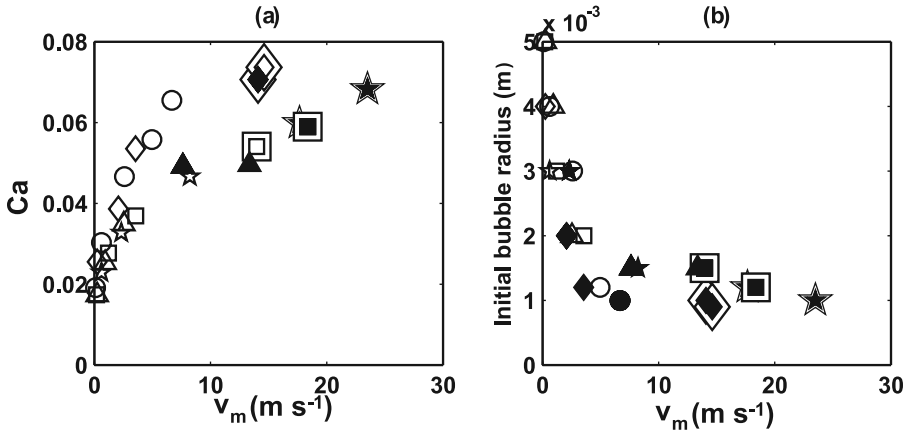

Figure 8. (a) Maximum capillary number calculated from equation (17) using averaged initial bubble radius as a function of maximum measured flow front velocity. Symbols used are the same as those in Figure 6, and solid symbols indicate that partial rupture is observed. (b) Required initial bubble radius to exceed Ca = 1 when decompression ends as a function of maximum measured flow front velocity. Symbols used are the same as those used in Figure 8a, but solid symbols indicate that deformation of bubbles is observed.

Capillary number and bubble film rupture or fragmentation is not obvious in Figure 8a, suggesting that fragmentation and bubble film rupture are not a result of deformation of bubbles.

[54] Figure 8b shows that the calculated minimum initial radius of bubbles needed to exceed Ca = 1. Ringed symbols indicate the experiments in which fragmentation is observed, and solid symbols show experiments in which visible deformation of bubbles is noted. As we can expect from equations (17) and (19), for faster flow front velocities, smaller bubbles can exceed Ca = 1. Among the experiments in which deformation of bubbles is visible, the maximum calculated radius needed to exceed Ca = 1 is 3 mm. In our experiments, a small number of bubbles up to this size (mostly smaller) are introduced when the fluid is poured into the high-pressure tube. These results suggest that bubble deformation may be restricted to initially large bubbles whose radii allow them to exceed Ca = 1.

4.2.4. A Regime Diagram

[55] Figure 9 summarizes the experimental results in a plot of enthalpy change $\Delta\hat{H}_{\mathrm{mod}}$ and the ratio of equilibrium and disequilibrium expansion velocities v_e/v_d. The equilibrium expansion velocity is given by equation (4), and the disequilibrium expansion velocity is calculated from equation (5).

[56] Figure 9 shows that when the equilibrium expansion velocity exceeds the disequilibrium one, several expansion styles can be observed, but when the disequilibrium expansion velocity exceeds the equilibrium one, the bubbly fluid can only expand. When inertia is dynamically important $\mathrm{Re}_c \gg 1$, overshoot is expected. The Reynolds number Re_c does not depend only on expansion velocity but also on the fluid density, so the threshold will not be defined by a sharp line.

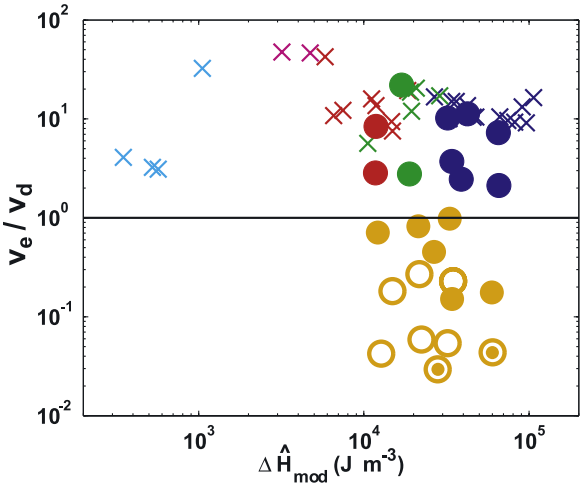

Figure 9. Regime diagram for experimental results. The x axis is the volumetric enthalpy change $\Delta\hat{H}_{\mathrm{mod}}$ calculated from equation (6); the y axis is the maximum ratio of equilibrium and disequilibrium expansion velocity v_e/v_d. Equilibrium v_e and disequilibrium v_d expansion velocities are calculated from equations (4) and (5), respectively. The velocity ratio varies during the decompression, and we plot the maximum value here. Circles show experiments conducted in this study, and crosses show experiments conducted in our previous study. Light blue, pink, red, green, dark blue, and orange indicate expansion styles of "nothing" happened, deformation is observed, detachment, partial rupture, fragmentation, and expansion, respectively. Solid symbols show the experiments in which overshoot occurs. The ringed circles are the experiments in which the occurrence of overshoot is ambiguous. Experimental set 1 for $R_{\mathrm{ori}} = 1/4$ is not plotted here. The black line indicates $v_e/v_d = 1$. To calculate v_e for experiments conducted in our previous work, we assume a uniform initial height of bubbly fluid column $h_{\mathrm{Fi}} = 0.05$ m because this height was not measured. For experiments in this work, we use the measured value.

5. Implications for Volcanic Eruptions

5.1. Critical Decompression Rate for the Disequilibrium Expansion

[57] The key result of our experiments is that there is an upper limit of the expansion velocity v_d if the decompression rate is high enough. In this limit, bubbles cannot

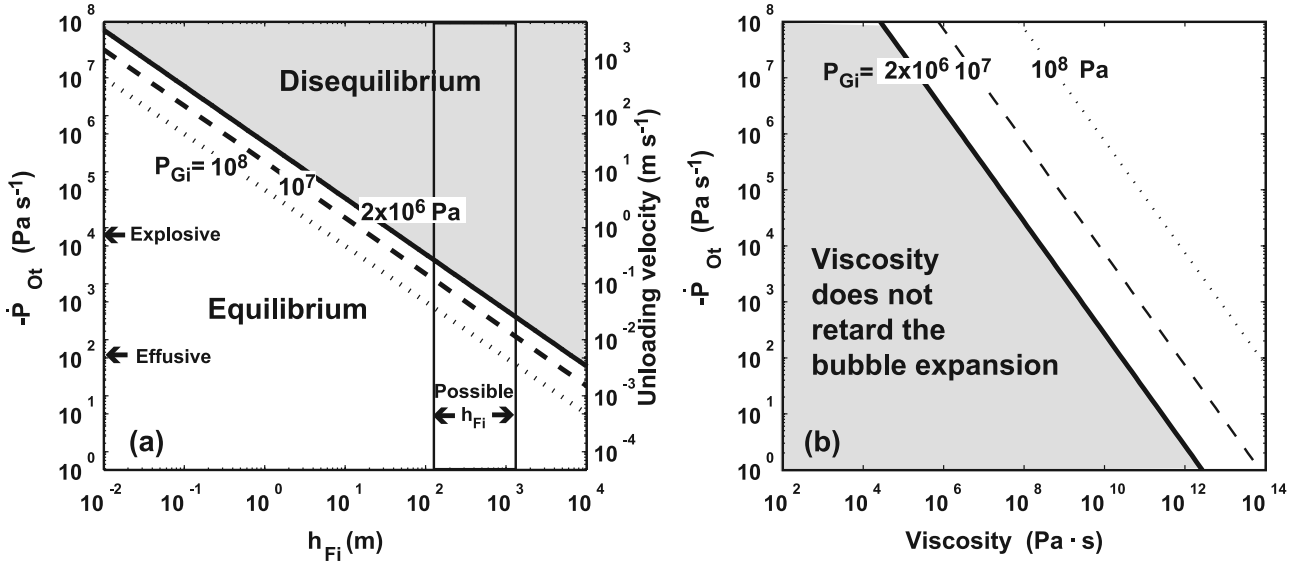

Figure 10. (a) Estimated decompression rate required for disequilibrium expansion calculated from equation (21), in which we assume $\phi_i = 0.5$, magma density $\rho_L = 2800$ kg m^{-3}, $P_{Ot} = 10^5$ Pa (atmospheric pressure), and $\gamma = 1.4$. Solid, dashed, and dotted lines show different initial pressure $P_{Gi} = 2 \times 10^6$, 10^7, and 10^8, respectively. Right-hand y axis shows the unloading velocity of magma corresponding to the decompression rate on left-hand y axis. The shaded regime indicates that fragmentation could occur. (b) Estimated upper limit viscosity for which viscosity does not hinder the bubble expansion calculated by equation (23). Each line corresponds to one shown in Figure 10a. We assume $P_{Of} = 10^5$ Pa.

expand fast enough to maintain the same pressure as that in the surrounding fluid. We now estimate the required decompression rate to cause disequilibrium expansion in magmas.

[58] Disequilibrium and equilibrium expansion velocities are given by equations (5), (6), and (4), respectively. In equation (6), when $P_{Ot} \ll P_{Gi}$, the terms that depend on P_{Ot} become much smaller than the terms that depend on P_{Gi}. For simplicity we can thus neglect the term involving P_{Ot} and approximate the enthalpy change as

$$\Delta \hat{H}_{mod} \approx \frac{\gamma \phi_i P_{Gi}}{\gamma - 1}. \tag{20}$$

The required decompression rate for $v_e > v_d$ is then given by

$$-\dot{P}_{Ot} > \left(\frac{2\gamma}{\rho_L \phi_i P_{Gi} (1 - \phi_i)(\gamma - 1)} \right)^{1/2} \frac{P_{Ot}^2}{h_{Fi}}. \tag{21}$$

Equation (21) depends on h_{Fi}^{-1}, and the required decompression rate becomes smaller as the height of the bubbly magma increases. This is because the equilibrium expansion velocity (equation (4)) depends on h_{Fi} and $\dot{P}_{Ot}$ but the disequilibrium expansion velocity (equation (5)), does not include these variables. Consequently, longer columns of the decompressed bubbly magma will experience disequilibrium expansion at lower decompression rates. In other words, making a larger volume bubbly fluid equilibrate to a new lower pressure requires a larger volume change.

[59] We now can calculate the required decompression rate for disequilibrium magma expansion. Figure 10a shows the threshold decompression rate for disequilibrium expansion for a range of heights of bubbly magma assuming $\phi_i = 0.5$. Figure 10a shows that the vertical length scale of the bubbly magma column affects the threshold decompression rate, as we noted in equation (21). The expansion of the longer bubbly magma column is in disequilibrium for lower decompression rates. Figure 10a also shows that the required decompression rate is lower for higher initial gas pressure P_{Gi}. This is because the equilibrium expansion velocity depends on the first power of initial gas pressure P_{Gi}, but the disequilibrium expansion velocity depends on the square root of the initial gas pressure $P_{Gi}^{1/2}$. As a consequence, larger initial pressure causes disequilibrium expansion with lower decompression rate.

[60] Another requirement for magma fragmentation is a sufficient initial pressure and vesicularity, $P_{Gi} > 10^6/\phi_i$ [*Spieler et al.*, 2004]. This condition is derived for rapid decompression. The thick line in Figure 10a assumes $P_{Gi} = 2 \times 10^6$ and $\phi_i = 0.5$. The shaded area indicates that the initial pressure exceeds this additional threshold and that the decompression rate exceeds the critical value for disequilibrium expansion, if both criteria are satisfied we predict that explosive eruption will result.

[61] When the viscosity of magma is sufficiently large and the decompression rate is high, the viscosity of the magma can retard bubble expansion. This effect is not taken into account in Figure 10a. We next estimate the viscosity range in which viscosity does not retard bubble expansion and the scaling shown in Figure 10a should apply. This viscosity range can be characterized by [*Thomas et al.*, 1994]

$$B = \frac{4\eta}{3 t_p \Delta P}, \tag{22}$$

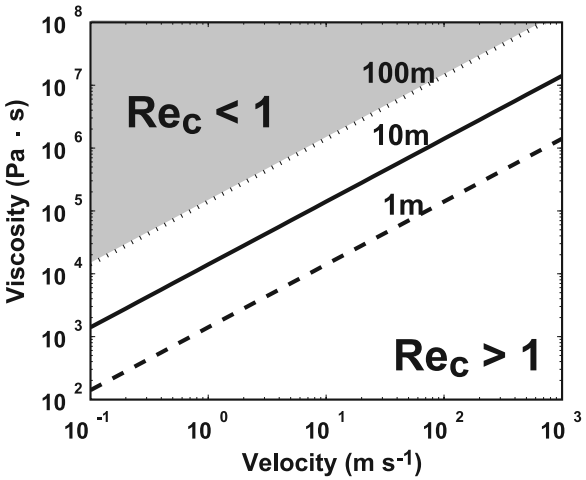

Figure 11. Estimated condition in which detachment could occur calculated by equation (12) to be $Re_c = 1$, in which density of magma and vesicularity are assumed as 2800 kg m^{-3} and 0.5, respectively. The conduit diameter is assumed to be 1, 10, and 100 m and is shown by dashed, solid, and dotted lines, respectively. Gray area indicates conditions for which detachment does not occur.

where B is a dimensionless variable that characterizes whether viscosity retards bubble expansion. When $B > 1$, viscous effects become significant. *Gardner et al.* [2000] confirm that this equation is consistent with decompression experiments with real magma.

[62] Using equation (22), we estimate the upper limit of viscosity for which the effect of viscosity can be neglected and our scaling would become relevant. Assuming that the decompression rate is constant, the upper limit viscosity is estimated by

$$\eta = \frac{3(P_{\mathrm{Gi}} - P_{\mathrm{Of}})^2}{-4\dot{P}_{\mathrm{Ot}}}. \tag{23}$$

Figure 10b shows the estimated upper limit viscosity for which viscosity does not affect bubble expansion. Each line corresponds to one of the lines in Figure 10a. In the shaded area, viscosity does not limit the expansion of bubbles. Viscosity of basalt is usually less than 100 Pa s [e.g., *Spera*, 2000], so the scaling shown Figure 10a should be appropriate for all basaltic eruptions. In the white region, viscosity retards bubble expansion and causes disequilibrium between the pressure inside and outside bubbles at lower decompression rates than calculated in Figure 10a. We thus apply Figure 10a to basaltic magma eruptions in the following.

[63] Explosive eruption of basaltic magma is sometimes attributed to the ascent of very vesicular magma, that is, a magma foam [e.g., *Parfitt*, 2004]. If exsolution of water during ascent generates the foam [*Wilson and Head*, 1981], the depth at which foam would originate depends on water content and an example for a Hawaiian eruption is 150 m [*Gerlach*, 1986]. Alternatively, a layer of foam could develop at the roof of a magma chamber [*Jaupart and Vergniolle*, 1988] at 1.5 km depth [*Allard et al.*, 2005]. We thus assume the height of the bubbly magma column is in the range of $10^2 - 10^3$ m.

[64] We estimate the decompression rate of basaltic eruptions using the unloading rate of the steadily erupting magma and by bubble number density, rather than the ascent rate of magma estimated by mineralogical methods, because the latter may reflect decompression rates at greater depths. *Vergniolle and Jaupart* [1986] compiled the magma flux and cross section area of conduits for many basaltic eruptions. Using these values, we can calculate an unloading velocity v_s between 10^{-3} and 10^{-2} m s^{-1} for effusive eruptions and 1 m s^{-1} for explosive eruptions. Assuming a vesicularity $\phi_i = 0.25$ [e.g., *Wolfe et al.*, 1989], the decompression equivalent to the unloading rate can be estimated by $\rho_M g v_s (1-\phi_i)$, where the subscript M indicates magma. Calculated decompression rates are between 20 and 200 Pa s^{-1} for effusive eruption and 2×10^4 Pa s^{-1} for explosive eruption.

[65] There are other techniques for estimating decompression rates, besides using estimates of conduit dimensions and mass fluxes. Decompression experiments have shown that the bubble number density depends on the decompression rate [*Gardner et al.*, 1999; *Mangan and Sisson*, 2000; *Mourtada-Bonnefoi and Laporte*, 2004]. *Toramaru* [2006] develops a method to calculate the decompression rate from bubble number density and obtains a decompression rate for subplinian eruption of basaltic magma in Izu Oshima $> 10^6$ Pa s^{-1}.

[66] From Figure 10a, we infer that our model is consistent with natural eruptions. Equilibrium expansion results when a bubbly magma column with vertical length between 10^2 and 10^3 m is decompressed at rate between 20 and 200 Pa s^{-1}, which are typical for effusive eruptions. On the other hand, disequilibrium occurs if the bubbly magma column decompressed at a rate of 2×10^4 Pa s^{-1}, which is the estimated decompression rate for explosive eruption. For higher decompression rates $>10^6$ Pa s^{-1}, a region of bubbly magma with a size <1 m may fragment.

5.2. Threshold for Detachment

[67] If detachment occurs it will influence eruptions by allowing exsolved gas in the conduit to escape. If the magma does not erupt from the conduit, this outgassed magma will be recycled within the conduit.

[68] Detachment, discussed in section 4.2.2, occurs when inertia exceeds the viscous drag; i.e., $Re_c \gg 1$. In Figure 11, we calculated this condition as a function of flow front velocity and viscosity. Figure 11 shows that when the viscosity is sufficiently low, detachment can occur. For example, even small parcels of magma with viscosity of 100 Pa s and expansion velocity of 1 m s^{-1} cannot stop by viscous drag. Again, viscosity for basaltic magma is usually less than 100 Pa s. We thus infer that detachment can occur for basaltic magma but should not occur for more viscous dacite and rhyolite magma.

[69] From Figure 11, we also can identify the regime in which our proposed framework applies. Under a rapid decompression, enthalpy changes are transferred to kinetic energy and determine the eruption velocity. In the white region, the inertial force is dominant so the assumption that enthalpy changes go into kinetic energy will be appropriate. On the other hand, in the shaded area, viscous drag can

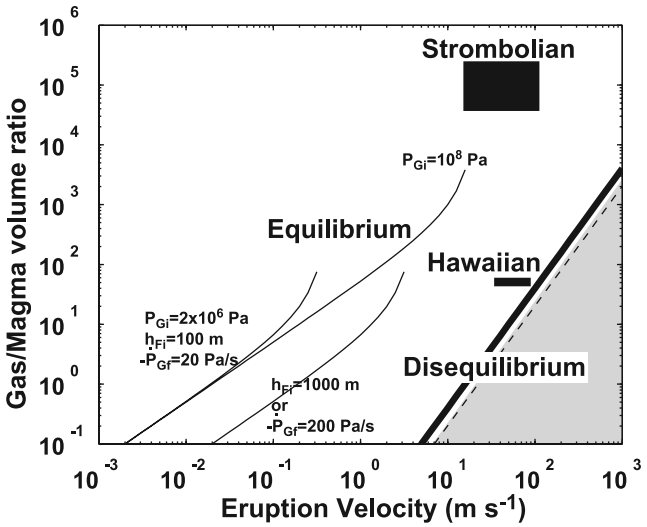

Figure 12. Predicted relation between volume ratio of gas and magma and eruption velocity. Solid thick line and dashed lines are disequilibrium expansion and are calculated by equations (28) and (29) assuming $\rho_M = 2800$ kg m^{-3}, $P_{Gf} = 10^5$ Pa, and $\gamma = 1.4$. For the dashed line, $P_{Gi} = 10^8$ Pa is assumed. Solid thin curves are for equilibrium expansion and are calculated by equation (30). Volume ratio and eruption velocity for Hawaiian and Strombolian eruption are estimated from data of *Greenland et al.* [1985], *Wolfe et al.* [1989], and *Chouet et al.* [1974].

decelerate the expansion of bubbly magma and the disequilibrium expansion velocity will be slower than that estimated by equation (5).

5.3. Ratio of the Gas and Magma

[70] In this section, we consider the relationship between the eruption velocity and the ratio of the volume of gas and magma to evaluate whether an eruption is caused by our proposed mechanism. If a bubbly magma ascends or is decompressed fast enough both partial rupture and fragmentation can occur and an explosive eruption results. For such an eruption, we can estimate the eruption velocity and the volume ratio of gas and magma. The relationship between these two values has been discussed frequently [e.g., *Vergniolle and Jaupart*, 1990; *Jaupart and Allegre*, 1991] and the basis of our analysis is similar to that of *Wilson* [1980] and *Wilson and Head* [1981].

[71] First, we consider the case in which the eruption velocity is based on adiabatic expansion, but the volume ratio of gas and magma is measured after thermal equilibration with surrounding magma. If the gas inside bubbles expands at a constant temperature, its volume change can be described as

$$P_{Gi} V_{Gi} = P_{Gf} V_{Gf}. \tag{24}$$

The initial vesicularity is given by

$$\phi_i = \frac{V_{Gi}}{V_M + V_{Gi}}, \tag{25}$$

where we neglect the volume change of the magma in this estimate. Eliminating V_{Gi} from equations (24) and (25), we obtain

$$\frac{1}{\phi_i} - 1 = \frac{P_{Gi}}{P_{Gf}} \frac{V_M}{V_{Gf}}. \tag{26}$$

[72] The scaling for the expansion velocity gives us another relation between initial pressure and vesicularity. When disequilibrium expansion occurs, the expansion velocity is given by equation (5) and $\Delta\hat{H}_{mod}$ can be approximated by equation (20). Approximating the bubbly magma density as $\rho_M(1-\phi_i)$, we obtain

$$\frac{1}{\phi_i} - 1 \approx \frac{\gamma P_{Gi}}{\gamma - 1} \frac{2}{\rho_M v_d^2}. \tag{27}$$

In equations (26) and (27), the relation between ϕ_i and P_{Gi} has a similar form. We thus can eliminate ϕ_i and P_{Gi} from these equations to obtain

$$\frac{V_{Gf}}{V_M} \approx \frac{\rho_M (\gamma - 1) v_d^2}{2\gamma P_{Gf}}. \tag{28}$$

An important feature of equation (28) is that the volume ratio of gas and magma depends on the square of eruption velocity.

[73] We can also calculate an analogous expression if the gas thermally equilibrates with the surrounding magma. In this case, equation (9) is appropriate for the eruption velocity. Using equations (26) and (9), ϕ_i can be eliminated and the relation between the eruption velocity and the volume ratio of gas and magma is

$$\frac{V_{Gf}}{V_M} \approx \frac{\rho_M v_d^2}{2P_{Gf}} \left\{ \ln\left(\frac{P_{Gi}}{P_{Gf}}\right) \right\}^{-1}. \tag{29}$$

[74] Assuming that the final gas pressure is atmospheric pressure, 10^5 Pa, we plot equations (28) and (29) in Figure 12 with solid thick and dashed lines, respectively. For the dashed line, $P_{Gi} = 10^8$ Pa is assumed. A line for equation (29) and $P_{Gi} = 2 \times 10^6$ Pa overlaps with the thick solid line. If observations fall on these lines, the eruption is likely the result of rapid expansion of bubbly magma. On the other hand, if it is not on these lines, another mechanism governs the eruption; e.g., exsolution of dissolved volatile species contributes to the eruption, isolated large bubbles expand, or a separation between the gas and magma occurs during the eruption. Although exsolution of dissolved volatile accelerates the eruption velocity, these effects are mainly expected to increase the observed volume ratio of gas and magma. Observations in the shaded regime are unexpected.

[75] We can also estimate the ratio of gas and magma for the equilibrium expansion case. The eruption velocity under equilibrium expansion is given by equation (4). Eliminating the vesicularity dependence by using equation (26), we obtain

$$\frac{V_{Gf}}{V_M} = \frac{v_e P_{Gf} P_{Gi}}{-\dot{P}_{Gf} P_{Gi} h_{Fi} - v_e P_{Gf}^2}. \tag{30}$$

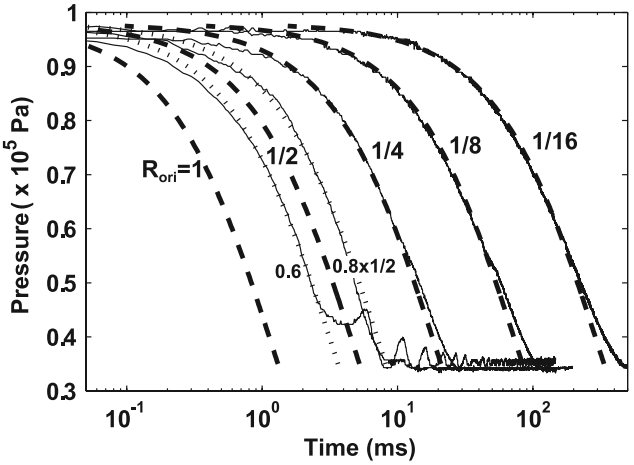

Figure A1. Measured and calculated pressure changes during decompressions with various orifice areas. Solid thin curves, from left to right, show measured values with the orifices R_{ori} = 1, 1/2, 1/4, 1/8, and 1/16, respectively. Dashed curves are calculated pressure changes using equation (A1) with R_{ori} = 1, 1/2, 1/4, 1/8, and 1/16, again from left to right. Dotted curves are calculated assuming that R_{ori} = 0.6 and 0.4. We assume that initial and final pressures are 9.8×10^4 and 3.5×10^4 Pa, respectively.

Equation (30) is shown with thin solid curves in Figure 12, in which we assume $P_{Gf} = 10^5$, $P_{Gi} = 2 \times 10^6$ Pa, $h_{Fi} = 100$ m, and $-\dot{P}_{Gf} = 20$ Pa s^{-1} for a reference case. The other two curves correspond to different values of P_{Gi}, h_{Fi} or $-\dot{P}_{Gf}$, where we note that changes in length scale h_{Fi} and the decompression rate $-\dot{P}_{Gf}$ are equivalent. These eruptions have lower eruption velocity and volume ratio of gas and magma than those for disequilibrium eruption. Because of the form of equation (30), the volume ratio of gas and magma becomes infinite when the eruption velocity reaches

$$v_e = -\frac{h_{Fi} P_{Gi}}{P_{Gf}^2} \dot{P}_{Gf}, \tag{31}$$

which occurs for an initial vesicularity $\phi_i = 1$. Such an initial condition is unrealistic, so each curve drawn for $\phi_i < 0.95$. If an effusive eruption occurs as a result of equilibrium expansion, the observed volume ratio of gas trapped in magma and magma should be fall on these thin curves. Different from the disequilibrium expansion, such the gas should not be released to the atmosphere, because of the absence of fragmentation and partial rupture.

[76] In Figure 12, we show two measured estimates of the volume ratio of gas and magma as a function of eruption velocity. For Hawaiian eruptions, *Greenland et al.* [1985] measured the weight fraction of magmatic gas degassed during episodes 15 and 16 Kilauea volcano, Hawaii in 1984. We calculate volume ratio of gas and magma from their data using the gas density of *Parfitt* [2004]. The eruption velocity is calculated from the fountain height H of episode 16 which is 60–400 m [*Wolfe et al.*, 1989] assuming $(2gH)^{1/2}$. For Strombolian eruptions, we use the data from *Chouet et al.* [1974].

[77] Hawaiian eruptions fall close to the line, suggesting that Hawaiian eruptions are mainly governed by the rapid decompression of bubbly magma. Strombolian eruptions plot well away from the line. Strombolian eruptions are usually attributed to the expansion and bursting of an isolated bubble [*Blackburn et al.*, 1976; *Wilson*, 1980] and are thus governed by different processes.

6. Conclusions

[78] On the basis of our experiments, we find two expansion velocities of bubbly fluid during decompression for the case in which viscosity does not influence bubble expansion. For slow decompression, equilibrium expansion occurs in which bubbly fluid expands to equilibrate the pressure inside the bubbles with that outside the bubbles. For fast decompression, disequilibrium expansion occurs in which bubbles expand with an upper limit velocity determined by the enthalpy change resulting from the decompression. Fragmentation and bubble film rupture can occur in this case. The threshold decompression rate for equilibrium/disequilibrium expansion is described by equation (21). This threshold depends on the length scale of the bubbly fluid column.

Appendix A: Calculating the Decompression Rate

[79] We estimate the decompression rate following the approach used by *Kieffer and Sturtevant* [1984]. The method assumes one-dimensional, quasi-steady compressible flow. The flow leaving the orifice is "choked" at the orifice because of the large pressure difference between the two tanks.

[80] The time-dependent pressure change P_{Ot} is

$$\left(\frac{P_{Ot}}{P_{Gi}}\right) = (Xt+1)^{2\gamma/(1-\gamma)}; \tag{A1}$$

$$X = \frac{c_0 A}{V_h}\left\{\left(\frac{\gamma-1}{2}\right)\left(\frac{2}{\gamma+1}\right)^{\frac{(\gamma+2)}{2(\gamma-1)}}\right\}, \tag{A2}$$

where P_{Gi} is initial pressure, γ is isentropic exponent, c_0 $\sim$345 m s^{-1} is sound velocity of dry air, A is the cross section area of exit flow and V_h is the volume of the high-pressure tube. An important feature of this equation is that a smaller exit flow area will lead to slower decompression. The duration of decompression t_p is estimated by

$$t_p = \frac{1}{X}\left\{\left(\frac{P_{Of}}{P_{Gi}}\right)^{(1-\gamma)/2\gamma} - 1\right\}. \tag{A3}$$

The decompression rate can thus be obtained from the time derivative of equation (A1)

$$\dot{P}_{Ot} = P_{Gi} X \frac{2\gamma}{1-\gamma}(Xt+1)^{\left(\frac{3\gamma-1}{1-\gamma}\right)}. \tag{A4}$$

[81] Figure A1 shows that for $R_{ori} \leq 1/4$, this model explains the measurements well. For $R_{ori} \geq 1/2$, however,

the measured decompression is slower than the calculated one. This can be attributed to the imperfect breakage of the diaphragms. When the orifice is large ($R_{ori} \geq 1/2$), the hole in the diaphragms might be smaller than the orifice.

[82] We calculate additional decompression curves for the cases $R_{ori} = 1$ and 1/2 with $A = A_h \times 0.6^2$ and $A = A_h \times (0.8/2)^2$, respectively, where A_h is the cross section area of the high-pressure tube. These curves are denoted in Figure A1 by dotted lines and explain the measurements well. However, the observed radius of the hole on the diaphragm is usually larger than 60% or 80% of the orifice radius. In these cases, because the response time of the transducer is 2 ms, which is almost the same as the decompression timescale when $R_{ori} = 1$, the real decompression rate is probably higher than the measured one. In this paper, we thus calculate the decompression rates without any correction for the ruptured diaphragm area and assume that the model in this appendix, in particular, equation (A4), is a reasonable approximation.

[83] **Acknowledgments.** We thank Helene Gaonac'h, James Gardner, and an anonymous reviewer for constructive comments. This work is supported by NSF. A.N. is supported by JSPS.

References

Alidibirov, M., and D. B. Dingwell (1996), Magma fragmentation by rapid decompression, *Nature*, *380*, 146–148.

Allard, P., M. Burton, and F. Mure (2005), Spectroscopic evidence for a lava fountain driven by previously accumulated magmatic gas, *Nature*, *433*, 407–410.

Barclay, J., D. S. Riley, and R. S. J. Sparks (1995), Analytical models for bubble growth during decompression of high viscosity magmas, *Bull. Volcanol.*, *57*, 422–431.

Blackburn, E. A., L. Wilson, and R. S. J. Sparks (1976), Mechanisms and dynamics of Strombolian activity, *J. Geol. Soc. London*, *132*, 429–440.

Burgisser, A., and J. E. Gardner (2005), Experimental constraints on degassing and permeability in volcanic conduit flow, *Bull. Volcanol.*, *67*, 42–56.

Carey, S., and H. Sigurdsson (1985), The May 18, 1980 eruption of Mount St. Helens: 2. Modeling of dynamics of the Plinian phase, *J. Geophys. Res.*, *90*, 2948–2958.

Chouet, B., N. Hamisevicz, and T. R. McGetchin (1974), Photoballistics of volcanic jet activity at Stromboli, Italy, *J. Geophys. Res.*, *79*, 4961–4976.

Devine, J. D., M. J. Rutherford, and J. E. Gardner (1998), Petrologic determination of ascent rates for the 1995–1997 Soufriere Hills Volcano andesitic magma, *Geophys. Res. Lett.*, *25*, 3673–3676.

Gaonac'h, H., S. Lovejoy, and D. Schertzer (2005), Scaling vesicle distributions and volcanic eruptions, *Bull. Volcanol.*, *67*, 350–357.

Gardner, J. E., M. Hilton, and M. R. Carroll (1999), Experimental constraints on degassing of magma: Isothermal bubble growth during continuous decompression from high pressure, *Earth Planet. Sci. Lett.*, *168*, 201–218.

Gardner, J. E., M. Hilton, and M. R. Carroll (2000), Bubble growth in highly viscous silicate melts during continuous decompression from high pressure, *Geochim. Cosmochim. Acta*, *64*, 1473–1483.

Gerlach, T. M. (1986), Exsolution of H_2O, CO_2, and S during eruptive episodes at Kilauea Volcano, Hawaii, *J. Geophys. Res.*, *91*, 12,177–12,185.

Geschwind, C. H., and M. J. Rutherford (1995), Crystallization of microlites during magma ascent: The fluid mechanics of 1980–1986 eruptions at Mount St. Helens, *Bull. Volcanol.*, *57*, 356–370.

Greenland, L. P., W. I. Rose, and J. B. Stokes (1985), An estimate of gas emissions and magmatic gas content from Kilauea Volcano, *Geochim. Cosmochim. Acta*, *49*, 125–129.

Hamley, I. W. (2000), *Introduction to Soft Matter: Polymers, Colloids, Amphiphiles and Liquid Crystals*, 250 pp. John Wiley, Hoboken, N. J.

Houghton, B., C. J. N. Wilson, P. D. Carlo, M. Coltelli, J. E. Sable, and R. Carey (2004), The influence of conduit processes on changes in style of basaltic Plinian eruptions: Tarawera 1886 and Etna 122 BC, *J. Volcanol. Geotherm. Res.*, *137*, 1–14.

Ichihara, M., D. Rittel, and B. Sturtevant (2002), Fragmentation of a porous viscoelastic material: Implications to magma fragmentation, *J. Geophys. Res.*, *107*(B10), 2229, doi:10.1029/2001JB000591.

Jaupart, C., and C. J. Allegre (1991), Gas content, eruption rate and instabilities of eruption regime in silicic volcanoes, *Earth Planet. Sci. Lett.*, *102*, 413–429.

Jaupart, C., and S. Vergniolle (1988), Laboratory models of Hawaiian and Strombolian eruptions, *Nature*, *331*, 58–60.

Kagiyama, T., H. Utada, and T. Yamamoto (1999), Magma ascent beneath Unzen Volcano, SW Japan, deduced from the electrical resistivity structure, *J. Volcanol. Geotherm. Res.*, *89*, 35–42.

Kieffer, S. W., and B. Sturtevant (1984), Laboratory studies of volcanic jets, *J. Geophys. Res.*, *89*, 8253–8268.

Klug, C., and K. V. Cashman (1996), Permeability development in vesiculating magmas: Implications for fragmentation, *Bull. Volcanol.*, *58*, 87–100.

Koyaguchi, T., and N. K. Mitani (2005), A theoretical model for fragmentation of viscous bubbly magmas in shock tubes, *J. Geophys. Res.*, *110*, B10202, doi:10.1029/2004JB003513.

Larsen, J. F., M. H. Denis, and J. E. Gardner (2004), Experimental study of bubble coalescence in rhyolitic and phonolitic melts, *Geochim. Cosmochim. Acta*, *68*, 333–344.

Lensky, N. G., O. Navon, and V. Lyakhovsky (2004), Bubble growth during decompression of magma: Experimental and theoretical investigation, *J. Volcanol. Geotherm. Res.*, *129*, 7–22.

Mader, H. M. (1989), Conduit flow and fragmentation, in *The Physics of Explosive Volcanic Eruptions*, edited by J. S. Gilbert and R. S. J. Sparks, *Geol. Soc. Spec. Publ.*, *145*, 51–71.

Mangan, M., and T. Sisson (2000), Delayed, disequilibrium degassing in rhyolite magma: Decompression experiments and implications for explosive volcanism, *Earth Planet. Sci. Lett.*, *183*, 441–455.

Martel, C., and B. C. Schmidt (2003), Decompression experiments as an insight into ascent rates of silicic magmas, *Contrib. Mineral. Petrol.*, *144*, 397–415.

Martel, C., D. B. Dingwell, O. Spieler, M. Pichavant, and M. Wilke (2000), Fragmentation of foamed silicic melts: an experimental study, *Earth Planet. Sci. Lett.*, *178*, 47–58.

Mastin, L. G. (1995), Thermodynamics of gas and steam-blast eruption, *Bull. Volcanol.*, *57*, 85–98.

Mastin, L. G. (1997), Evidence for water influx from a caldera lake during the explosive hydromagmatic eruption of 1790, Kilauea Volcano, Hawaii, *J. Geophys. Res.*, *102*, 20,093–20,109.

Mourtada-Bonnefoi, C. C., and D. Laporte (2004), Kinetics of bubble nucleation in a rhyolitic melt: An experimental study of the effect of ascent rate, *Earth Planet. Sci. Lett.*, *218*, 521–537.

Nakada, S., Y. Motomura, and H. Shimizu (1995), Manner of magma ascent at Unzen Volcano (Japan), *Geophys. Res. Lett.*, *22*, 567–570.

Namiki, A., and M. Manga (2005), Response of a bubble bearing viscoelastic fluid to rapid decompression: Implications for explosive volcanic eruptions, *Earth Planet. Sci, Lett.*, *236*, 269–284.

Parfitt, E. A. (2004), A discussion of the mechanisms of explosive basaltic eruptions, *J. Volcanol. Geotherm. Res.*, *134*, 77–107.

Proussevitch, A. A., and D. L. Sahagian (1996), Dynamics of coupled diffusive and decompressive bubble growth in magmatic systems, *J. Geophys. Res.*, *101*, 17,447–17,455.

Rutherford, M. J., and J. D. Devine (2003), Magmatic conditions and magma ascent as indicated by hornblende phase equilibria and reactions in the 1995–2002 Soufriere Hills magma, *J. Petrol.*, *44*, 1433–1454.

Rutherford, M. J., and J. E. Gardner (2000), Rates of magma ascent, in *Encyclopedia of Volcanoes*, edited by H. Sigurdsson, pp. 207–217, Elsevier, New York.

Rutherford, M. J., and P. M. Hill (1993), Magma ascent rates from amphibole breakdown: An experimental study applied to the 1980–1986 Mount St. Helens eruptions, *J. Geophys. Res.*, *98*, 19,667–19,685.

Saar, M. O., and M. Manga (1999), Permeability-porosity relationship in vesicular basalts, *Geophys. Res. Lett.*, *26*, 111–114.

Scandone, R., and S. D. Malone (1985), Magma supply, magma discharge and readjustment of the feeding system of Mount St. Helens during 1980, *J. Volcanol. Geotherm. Res.*, *23*, 239–262.

Self, S., L. Wilson, and I. A. Nairn (1979), Vulcanian eruption mechanisms, *Nature*, *277*, 440–443.

Sheridan, M. F., and K. H. Wohletz (1983), Hydrovolcanism—Basic considerations and review, *J. Volcanol. Geotherm. Res.*, *17*, 1–29.

Spera, F. J. (2000), Physical properties of magma, in *Encyclopedia of Volcanoes*, edited by H. Sigurdsson, pp. 171–190, Elsevier, New York.

Spieler, O., B. Kennedy, U. Kueppers, D. B. Dingwell, B. Scheu, and J. Taddeucci (2004), The fragmentation threshold of pyroclastic rocks, *Earth Planet. Sci. Lett.*, *226*, 139–148.

Thomas, N., C. Jaupart, and S. Vergniolle (1994), On the vesicularity of pumice, *J. Geophys. Res.*, *99*, 15,633–15,644.

Toramaru, A. (1995), Numerical study of nucleation and growth of bubbles in viscous magmas, *J. Geophys. Res.*, *100*, 1913–1931.

Toramaru, A. (2006), BND (bubble number density) decompression rate meter for explosive volcanic eruptions, *J. Volcanol. Geotherm. Res.*, *154*, 303–316.

Vergniolle, S., and C. Jaupart (1986), Separated two-phase flow and basaltic eruptions, *J. Geophys. Res.*, *91*, 12,842–12,860.

Vergniolle, S., and C. Jaupart (1990), Dynamics of degassing at Kilauea Volcano, Hawaii, *J. Geophys. Res.*, *95*, 2793–2809.

Vergniolle, S., and M. Mangan (2000), Hawaiian and Strombolian eruptions, in *Encyclopedia of Volcanoes*, edited by H. Sigurdsson, pp. 447–461, Elsevier, New York.

Walker, G. P. L., S. Self, and L. Wilson (1984), Tarawera 1886, New Zealand—A basaltic Plinian fissure eruption, *J. Volcanol. Geotherm. Res.*, *21*, 61–78.

Wilson, L. (1980), Relationship between pressure, volatile content and ejecta velocity in three types of volcanic explosion, *J. Volcanol. Geotherm. Res.*, *8*, 297–313.

Wilson, L., and J. W. Head (1981), Ascent and eruption of basaltic magma on the Earth and Moon, *J. Geophys. Res.*, *86*, 2971–3001.

Wolfe, E. W., M. O. Garcia, D. B. Jackson, R. Y. Koyanagi, C. A. Neal, and A. T. Okamura (1989), The Puu Oo eruption of Kilauea volcano, episodes 1–20, January 3, 1983, to June 8, 1984, *U. S. Geol. Surv. Prof. Pap., 1350*, 471–508.

Woods, A. W., and T. Koyaguchi (1994), Transitions between explosive and effusive eruptions of silicic magmas, *Nature*, *370*, 641–644.

Yamada, K., H. Tanaka, K. Nakazawa, and H. Emori (2005), A new theory of bubble formation in magma, *J. Geophys. Res.*, *110*, B02203, doi:10.1029/2004JB003113.

Zhang, Y. (1999), A criterion for the fragmentation of bubbly magma based on brittle failure theory, *Nature*, *402*, 648–650.

M. Manga, Department of Earth and Planetary Science, University of California Berkeley, 307, McCone Hall, Berkeley, CA 94720-4767, USA. (manga@seisemo.berkeley.edu)

A. Namiki, Institute of Geology and Geoinformation, Magma Activity Research Group, Higashi 1-1-1 AIST no. 7, Tsukuba 305-8567, Japan. (namiki-atsuko@aist.go.jp)